Mechanism of smart baroreception in the aortic arch

G. C. Kember,[1] J. A. Armour,[2] and M. Zamir[3]
[1]*Department of Engineering Mathematics, Dalhousie University, P. O. Box 1000, Halifax, Nova Scotia, Canada, B3J 2X4*
[2]*Department of Pharmacology, University of Montréal, Montréal, Québec, Canada, H3C 3J7*
[3]*Departments of Applied Mathematics and of Medical Biophysics, University of Western Ontario, London, Ontario, Canada, N6A 5B7*
(Received 13 January 2006; published 25 September 2006)

A mechanism is proposed by which the patch of baroreceptors along the inner curvature of the arch of the aorta can sense hemodynamic events occurring downstream from the aortic arch, in the periphery of the arterial tree. Based on a solution of equations governing the elastic movements of the aortic wall, it is shown that the pressure distribution along the patch of baroreceptors has the same functional form as the distribution of strain along the patch. The significance of these findings are discussed, particularly as they relate to the possibility of a neuromechanical basis of essential hypertension.

DOI: 10.1103/PhysRevE.74.031914 PACS number(s): 87.19.Hh

I. INTRODUCTION

Cardiovascular control is dependent upon feedback arising from sensors, the afferent neurons, distributed throughout the cardiopulmonary system which serve to transduce regional mechanical and chemical events [1]. These sensory neurons provide feedback to the cardiovascular neuronal hierarchy of the mechanical state and chemical milieu of various cardiac and vascular tissues. One of the major sources of such information is provided by arterial baroreceptors. The mechanism of arterial baroreception involves the transduction of pressure by mechanosensory neurites to an associated barosensory neuron [2,3]. Much of our information concerning the physiology of arterial baroreception has been derived from studies focusing on the function of individual baroreceptor neurons concentrated in the carotid bulb because of their relative accessibility and consistency of response [4]. For complementary reasons, fewer studies have focused on mechanosensory neurons that transduce *aortic* pressure.

The sensory neurites associated with afferent neurons that transduce aortic pressure are continuously distributed along the inner aortic arch [5]. As their somata are adjacent to the heart, they are capable of originating short-latency reflex control of cardiac motor neurons [1]. Based on their anatomical and functional properties, these mechanosensory neurons are capable of transducing more complex information than mechanosensory neurons in the carotid bulb which are confined to "point" arterial baroreception. Specifically, aortic pressure transduction is achieved by a distributed array of multiple mechanosensory fields spread along the inner curvature of the aortic arch. They are close to neurons in ganglia adjacent to the aortic arch, i.e., mediastinal, middle cervical, and stellate ganglia. Due to their proximity, they are capable of relaying local aortic wall dynamics rapidly and accurately to motor neurons involved in cardiac regulation [1]. In addition, this sensory collective can also transduce and rapidly update spatial snapshots of perturbations of the aortic wall caused by wave reflections coming from downstream. These are accumulated wave reflections that arise as the propagating pulsatile flow encounters the large number of branching sites downstream. It was shown in Ref. [3] that these downstream events affect, indeed determine, the pressure distribution along the aortic arch that is sensed by the array of neurons along the aortic arch wall. The phenomenon was termed "smart" baroreception in the sense that the information being transduced is more than just local (point) pressure, but also pressure distribution.

What must be determined next is the mechanism by which smart baroreception actually occurs. More specifically, (i) how is the pressure distribution along the wall of the aortic arch translated into an input signal for the array of the baroreceptors and (ii) how is this input signal processed to produce an output signal for the regulatory system. The present paper is devoted to these two questions.

The ultimate goal of this work is an understanding of the neural regulation of aortic blood throughput under normal circumstances, with a view to exploring the possibility of a neuromechanical basis for the evolution of essential hypertension.

II. AORTIC WALL STRETCH

A localized change in pressure within the aortic arch causes a localized stretch which serves as the input signal to a baroreceptor at that location, and changes in this signal are then interpreted as changes in pressure. Now, a *strip* of sensory neurons along the arch of the aorta will sense not only local stretch but also the *distribution* of stretch along the patch of the aortic wall which the strip covers. For this reason, in what follows, we consider stretch to be a *function of position* along the aortic wall. In pulsatile flow, of course, stretch is also a function of time, but this feature will be considered later.

Consider a small segment of the sensory strip along the arch of the aorta, the latter being modeled as a tube whose radius in the absence of stretch is a. While this assumption is a clear idealization, the analysis to follow is based on only a small segment of the surface of the aorta and hence the approximation involved is not unreasonable. The principal issue in smart baroreception is the sensing of a *distribution* of pressure along a strip of the aortic wall as opposed to the sensing of pressure at a single point. The small curvature of the strip caused by curvature of the aortic arch is therefore only a secondary issue.

 ©2006 The American Physical Society

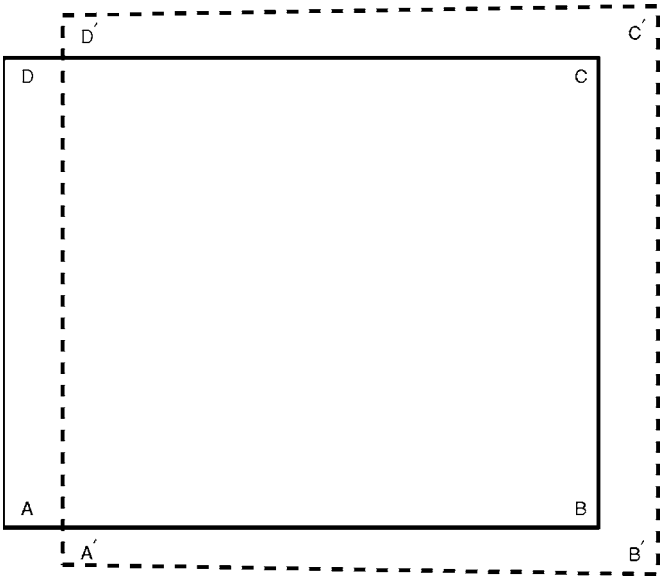

FIG. 1. A small rectangular segment of the sensory strip along the inner wall of the arch of the aorta which is being modeled as a tube, using cylindrical polar coordinates x, r, θ in the axial, radial, and circumferential directions, respectively. In the unstretched state the radius of the tube is a, and if the coordinate position of corner A of the rectangular segment is (x, a, θ), then the position of corner C is $(x+\delta x, a, \theta+\delta\theta)$. In the stretched state the new positions A', C' of the same two corners are $[x+\xi(x), a+\eta(x), \theta]$ and $[x+\delta x+\xi(x+\delta x), a+\eta(x+\delta x), \theta+\delta\theta]$.

If the length, in the axial direction, of the small segment of the sensory strip is δx and the angle which it subtends in the circumferential direction is $\delta\theta$, then its surface area as shown in Fig. 1 is

$$A = a\,\delta\theta\delta x. \tag{1}$$

Because the amount of stretch within this small surface area will vary from point to point, it is convenient to express it in terms of the displacements of each material point within the surface area being considered. In the process of stretching, a point is displaced by an amount ξ in the axial direction and η in the radial direction. Displacements in the circumferential direction are considered zero on the assumption of axial symmetry.

In order to account for changes in pressure and hence changes in the amount of stretch in the axial direction, the axial and radial displacements ξ, η must be considered functions of x. Thus, following a radial displacement $\eta(x)$ and axial displacement $\xi(x)$, the change in the surface area of the segment being considered, to be denoted by δA, is given by

$$A + \delta A = \{[x + \delta x + \xi(x + \delta x)] - [x + \xi(x)]\} \times \left\{\frac{[a + \eta(x)] + [a + \eta(x + \delta x)]}{2}\right\}\delta\theta. \tag{2}$$

For small displacements, and using Eq. (1), we find

$$\delta A \approx (a\,\delta\theta\delta x)\left\{\left(1 + \frac{\partial\xi}{\partial x}\right)\left(1 + \frac{\eta}{a}\right) - 1\right\}. \tag{3}$$

Equation (3) gives the local stretch as a function of the local displacements $\xi(x)$, $\eta(x)$, and the local gradient of ξ. The local *strain* e is defined as

$$e(\xi, \eta, t) = \frac{\delta A}{A}, \tag{4}$$

and using Eqs. (1)–(3) this becomes

$$e(\xi, \eta, t) = \left(1 + \frac{\partial\xi}{\partial x}\right)\left(1 + \frac{\eta}{a}\right) - 1, \tag{5}$$

which for small displacements, finally reduces to

$$e(\xi, \eta, t) \approx \frac{\partial\xi}{\partial x} + \frac{\eta}{a}. \tag{6}$$

The range of validity of this approximation is established at the end of Sec. IV.

III. AORTIC WALL MOTION

Motion of the aortic wall is driven by the shear stress τ_w exerted by the moving fluid on the inner surface of the vessel and by the pressure p_w acting on the same surface. Since our interest is in the response of baroreceptors to changes in pressure, in what follows we take p_w as the only driving force, which is equivalent to considering the flow as being inviscid since the wall shear stress is being neglected. Treating the flow as inviscid has the advantage of isolating the effects of wave reflections from the effects of viscosity, which are known to merely reduce the wave amplitude and wave speed in a reasonably predictable fashion. A major benefit of this is that the coupling between the wall motion and flow field equations is simplified. An analytic solution can be obtained for the wall motion equations with a clear description of the main elements of baroreceptor function as we show below.

Assuming that the tube wall is elastic and is characterized by Young's modulus E and Poisson's ratio σ, the wall motion is governed by the equations of elasticity [6]

$$\frac{\partial^2\xi}{\partial t^2} = \frac{E}{\rho_w}\left(\frac{\partial^2\xi}{\partial x^2} + \frac{\sigma}{a}\frac{\partial\eta}{\partial x}\right) - \frac{\tau_w}{\rho_w h}, \tag{7}$$

$$\frac{\partial^2\eta}{\partial t^2} = \frac{p_w(x,t)}{\rho_w h} - \frac{E}{\rho_w a}\left(\frac{\eta}{a} + \sigma\frac{\partial\xi}{\partial x}\right), \tag{8}$$

where τ_w is the shear stress between the wall and the moving fluid. It is convenient to put these equations in nondimensional form by writing

$$\bar{\xi} = \frac{\xi}{a}, \quad \bar{\eta} = \frac{\eta}{a}, \quad X = \frac{x}{a}, \tag{9}$$

$$T = \sqrt{\frac{E}{\rho_w a^2}}\,t, \quad P = \frac{a}{Eh}p_w, \quad \bar{\tau}_w = \frac{a\tau_w}{Eh}, \tag{10}$$

whereby Eq. (7) and Eq. (8) become

$$\frac{\partial^2 \bar{\xi}}{\partial T^2} = \frac{\partial^2 \bar{\xi}}{\partial X^2} + \sigma \frac{\partial \bar{\eta}}{\partial X} - \bar{\tau}_w, \tag{11}$$

$$\frac{\partial^2 \bar{\eta}}{\partial T^2} = P(X,T) - \bar{\eta} - \sigma \frac{\partial \bar{\xi}}{\partial X}. \tag{12}$$

To assess the order of magnitude of the dimensionless shear stress $\bar{\tau}_w$ we use the expression for shear stress in steady flow [6] $\tau_w = 4\mu q/\pi a^3$ which on substitution in Eq. (10) gives $\bar{\tau}_w = 4\mu q/\pi a^2 Eh$. Taking parameter values appropriate for the human cardiovascular system, (i) Young's modulus $E \approx 10^7$ g/cm s^2, (ii) aortic radius $a \approx 1$ cm and diameter $d \approx 2$ cm, (iii) aortic wall thickness $h \approx 0.2$ cm, (iv) $\mu \approx 0.04$ g/cm s, and (v) $q \approx 5$ l/min ≈ 100 cm^3/s. We find $\bar{\tau}_w \approx 10^{-5}$. On this basis, the shear term in Eq. (11) can clearly be neglected.

Neglecting the wall shear stress, the movement of the wall is thus seen to be driven by the pressure distribution along the wall, or more accurately by the form of $p_w(x,t)$ in Eqs. (7) and (8) or, in nondimensional terms, by the form of $P(X,T)$ in Eq. (12). In the presence of wave reflections, the first of these is given by [6]

$$p_w(x,t) = p_0 e^{i\omega t}(e^{-i\omega x/c_0} + Re^{i\omega(x-2l)/c_0}), \tag{13}$$

where p_0 is a constant, ω is the frequency of the oscillatory flow under which wave reflections are taking place, l is the length of a tube segment under consideration, and x is axial coordinate within that segment such that $x=0$ is the entrance and $x=l$ is a reflection site downstream at which R is the reflection coefficient.

In the branching tree structure of the aorta, the tube segment under consideration is a segment of the aortic arch, and the reflection coefficient R in Eq. (13) then represents the cumulative effects of wave reflections from all branches of the aorta downstream of that segment. In order to solve Eqs. (7) and (8) with p_w as prescribed in Eq. (13), it is convenient to put the latter in nondimensional form by introducing

$$\bar{p}_0 = \frac{a}{Eh} p_0, \quad \bar{R} = Re^{-i2\omega l/c_0}, \quad \lambda = \sqrt{\frac{\rho_w a^2}{E}}\omega, \quad \Lambda = \frac{\omega a}{c_0}, \tag{14}$$

whereby Eq. (13) becomes

$$P(X,T) = \bar{p}_0 e^{i\lambda T}\{e^{-i\Lambda X} + \bar{R}e^{i\Lambda X}\}. \tag{15}$$

IV. WALL STRAIN DISTRIBUTION

The local strain function $e(\xi, \eta, t)$ in Eq. (6) defines the distribution of strain along the aortic wall in terms of the local displacements ξ, η and time t. For a given form of the pressure distribution along the aortic wall, these displacements become functions of position along the wall, the nature of these functions being determined from a solution of Eqs. (7) and (8) or Eqs. (11) and (12). We thus define the following wall *strain distribution function*,

$$S(X,T) = e\{\xi(X,T), \eta(X,T), t(T)\}, \tag{16}$$

which upon using Eq. (6) becomes

$$S(X,T) \approx \frac{\partial \bar{\xi}(X,T)}{\partial X} + \bar{\eta}(X,T), \tag{17}$$

and what remains is to solve Eqs. (11) and (12) for the displacement functions $\bar{\xi}(X,T), \bar{\eta}(X,T)$.

Now, solving Eqs. (11) and (12) using the pressure distribution in Eq. (15) gives

$$\bar{\xi}(X,T) = A\bar{p}_0 e^{i\lambda T}\{e^{-i\Lambda X} + \bar{R}e^{i\Lambda X}\}, \tag{18}$$

$$\bar{\eta}(X,T) = B\bar{p}_0 e^{i\lambda T}\{e^{-i\Lambda X} + \bar{R}e^{i\Lambda X}\}, \tag{19}$$

where A, B are constants given by

$$A = \frac{i\Lambda\sigma}{(\Lambda^2 - \lambda^2)(1-\lambda^2) - \Lambda^2\sigma^2}, \tag{20}$$

$$B = \frac{\Lambda^2 - \lambda^2}{(\Lambda^2 - \lambda^2)(1-\lambda^2) - \Lambda^2\sigma^2}. \tag{21}$$

Substituting these results in Eq. (16) then gives

$$S(X,T) \approx \frac{\partial \bar{\xi}(X,T)}{\partial X} + \bar{\eta}(X,T) \tag{22}$$

$$= \left(\frac{\Lambda^2(1-\sigma) - \lambda^2}{(\Lambda^2 - \lambda^2)(1-\lambda^2) - \Lambda^2\sigma^2}\right)\bar{p}_0 e^{i\lambda T}\{e^{-i\Lambda X} + \bar{R}e^{i\Lambda X}\}. \tag{23}$$

Comparing this result for the strain distribution $S(X,T)$ with the result for the pressure distribution $P(X,T)$ in Eq. (15) indicates that the two distributions are precisely the same functions of position and time, that is

$$S(X,T) \sim P(X,T). \tag{24}$$

This remarkable result shows clearly that the pressure distribution along the arch of the aorta, as modified by wave reflections from downstream, translates directly into the signal transduced by the patch of baroreceptors in the process of what has been called "smart" baroreception.

The result in Eq. (24) depends on the underlying assumption in Eq. (6) that the product $(\partial\xi/\partial x)(\eta/a)$, which was neglected on the right-hand side of that equation, is small compared with the sum $(\partial\xi/\partial x + \eta/a)$ which was retained, i.e.,

$$\left(\frac{\partial \xi}{\partial x}\right)\left(\frac{\eta}{a}\right) \ll \frac{\partial \xi}{\partial x} + \frac{\eta}{a}. \tag{25}$$

To test this assumption we show first that by using parameter values as before, along with Poisson's ratio $\sigma \approx 0.5$, blood density $\rho \approx 1$ g/cm^3, wall density $\rho_w \approx 1$ g/cm^3, oscillatory flow circular frequency $\omega \approx 10$, wave speed from the Moen-Korteweg formula $c_0 = \sqrt{Eh/\rho d} \approx 1000$ cm/s, and the constant pressure $p_0 \approx 10^4$ g/cm/s^2 corresponding to

10 mm Hg, the right-hand sides of Eqs. (22) and (23), in dimensional form, yield

$$\frac{\partial \xi}{\partial x} + \frac{\eta}{a} \approx 0.1. \tag{26}$$

Since it is assumed that the relative change in η/a is small, it follows from Eq. (26) that $\partial\xi/\partial x$ must also be small. It follows finally therefore that the product of $\partial\xi/\partial x$ and η/a is smaller than their sum as required in Eq. (25).

There are clearly circumstances where the small displacement approximation does fail. However, in the present study our focus is on circumstances associated with essential hypertension which involve only a small chronic rise in blood pressure and hence the small displacement approximation would not be violated.

V. SIGNAL PROCESSING REQUIREMENTS

So far, we have shown that smart baroreception can produce a signal describing the pressure distribution along a patch of the aortic arch wall in terms of stretch distortions along the patch, and that the exact form of this signal is affected by hemodynamic events downstream. What remains to be determined is the extent to which the signal processing capability of the system is physically matched to the level of wall distortions typically produced.

In humans, the aortic sensory array extends about 150 mm in the axial direction along the inner curvature of the arch while encompassing about 40% of the arch in the circumferential direction and yielding a total sensory area of around 500 mm^2 [5]. Each field or "member" of the array is approximately elliptical and covers an area about 1 mm^2, with its major axis oriented in the aortic axial direction [5].

Each array member responds to local aortic wall distortion and supplies inputs to its associated A-δ fiber. These inputs cause the A-δ fiber to produce action potentials at rates ranging from about 10 to 100 Hz. Each action potential is relayed a short distance of about 1 to 5 cm at a speed of approximately 10 m/s into the sympathetic neural hierarchy [12]. The short transmission distance and high conduction speed allow the A-δ fibers to influence fast cardiac reflexes with transmission delays limited to only 0.01 s or so.

From a signal processing point of view, each instantaneous change in the A-δ firing rate or time between all-or-none action potentials represents a single sample of the aortic wall distortion. It is in this sense that the analog aortic wall distortion signal is being "digitally sampled" by the A-δ fiber via its action potentials. This is illustrated in Fig. 2 where the data marked "Window" represent baroreceptor transduction of the local "Aortic Pressure" data shown in the same figure. It is seen that the time between spikes in the window data is clearly sensitive to aortic pressure levels and there is little phase lag in their response to changes in aortic pressure.

Smart baroreception "senses" the pressure distribution along the array of baroreceptors by having members of the array digitally sample the wall distortions at their respective location, the results being converted to pressure according to Eq. (24). For this process to succeed the digital sampling

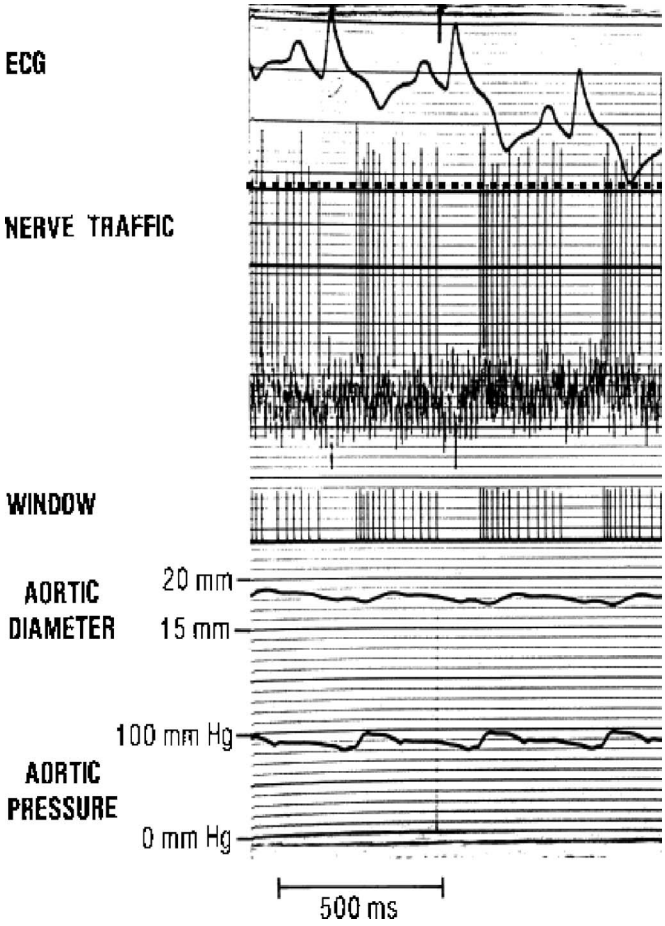

FIG. 2. Neural activity generated by one canine aortic mechanoreceptor, along with simultaneous measurements of aortic diameter and pressure from the same region. Shown are measured electrocardiogram (ECG), measured afferent neuron activity (Nerve Traffic), window discriminated afferent neuron activity (Window), measured aortic diameter (Aortic Diameter), and measured aortic pressure (Aortic Pressure). Action potential peaks in the nerve traffic data panel above the heavy dashed line have been set to unity and the signal is otherwise zeroed. Measured aortic pressure levels show a close inverse correlation with time between spikes in the window discriminated afferent neuron activity.

regime must be compatible with the analog wall distortion data which in turn depends on the degree to which the wave reflections returning from downstream are resolved in space and time. This is because the pressure distribution in pulsatile flow in an elastic tube segment is made up of the combined amplitudes of the harmonics of forward and backward waves in that segment [6]. The pressure distribution along the patch of baroreceptors in the aortic arch is therefore strongly dependent on the extent of wave reflections from downstream.

Resolution of the aortic wave in time depends on the wave's period T and hence on the corresponding frequency f. The maximum frequency component within the aortic wave that must be resolved is $f \approx 10$ Hz, or a period $T \approx 0.1$ s [7]. Accordingly, the Nyquist sampling theorem requires a minimum of two samples per period to resolve a given period and an A-δ fiber firing at 20 Hz can resolve an $f = 10$ Hz analog

signal. Thus, very high resolution of an $f=10$ Hz signal is achieved when an A-δ fiber fires at 100 Hz, since 100 Hz corresponds to five times the Nyquist-limit or ten samples per period of oscillation. In Fig. 2, the highest A-δ firing rates seen in the "Window" data, estimated by counting the number of spikes per second, range from 40 to 80 Hz. This corresponds to a fairly high resolution of the "Aortic Pressure" variations seen near the $f=10$ Hz upper limit with 4 to 8 samples per 0.1 s period.

Resolution of the aortic wave in space depends on the prevailing wave length and hence on the corresponding wave speed c. An estimate of the wave speed is given by the Moen-Korteweg approximation whereby $c \approx \sqrt{Eh/\rho d}$ [8–11], where E is the elasticity, h is thickness, d is diameter of the aortic wall, and ρ is fluid density. In the human aorta $E \approx 10^7$ g/cm/s^2, $h \approx 0.2$ cm, $\rho \approx 1$ g/cm^3, and $d \approx 2$ cm which taken together give $c \approx 10$ m/s [13].

The shortest space interval that must be resolved is therefore given by the product of wave speed $c \approx 10$ m/s and the shortest period $T \approx 0.1$ s. Hence, the wavelength of a 10 Hz wave traveling at about 10 m/s within the aorta is approximately 1 m. Such a long space interval is easily resolved by the array of baroreceptors since its length of 150 mm extends over only 15% of the 1 m wavelength. This means that only a small part of the wave is being sampled by the patch of baroreceptors, which leads to a nearly linear variation in pressure over the length of the patch [7] and a resolution of only the local value and slope of the pressure distribution over the smart baroreceptor domain.

VI. DISCUSSION

The concept of smart baroreception proposes that the patch of baroreceptors along the inner curvature of the arch of the aorta is capable of sensing not only local pressure as in a single baroreceptor, but also the pressure *distribution* along the patch. Since the pressure distribution is strongly affected by wave reflections returning from the periphery of the aortic arterial tree [7], the concept of smart baroreception proposes in effect that the patch of baroreceptors in the aortic arch is capable of sensing hemodynamic events occurring downstream from the arch, in the periphery of the arterial tree.

In this paper we have shown that the principal *mechanism* of smart baroreception is actually based on the remarkable result that the pressure distribution along the patch of baroreceptors has the same functional form as the distribution of strain along the same patch. The result follows from a solution of equations governing the elastic movements of the aortic wall. With strain being the mediating input signal in the baroreception process, we have shown further that the required resolution of this signal is well within the signal processing capability of the system.

The significance of these findings lies in the neural regulation of blood flow and cardiovascular control. In particular, they offer a possible *neuromechanical* basis for the pathogenesis of essential hypertension whereby the progression of the disease is seen as a gradual remodeling of neural control of cardiovascular function due to structural changes in the aortic arch and/or the downstream arterial tree.

[1] J. A. Armour and G. C. Kember, *Basic and Clinical Neurocardiology*, edited by J. A. Armour and J. L. Ardell (Oxford University Press, New York, 2003).
[2] M. C. Andresen, J. M. Krauhs, and A. M. Brown, Circ. Res. **43**, 728 (1978).
[3] P. Thoren, W. R. Saum, and A. M. Brown, Circ. Res. **40**, 231 (1977).
[4] M. C. Andresen and D. L. Kunze, Annu. Rev. Physiol. **56**, 93 (1994).
[5] J. A. Armour, Am. J. Physiol. **225**, 177 (1973).
[6] M. Zamir, *The Physics of Pulsatile Flow* (Springer-Verlag, New York, 2000).
[7] G. Kember, J. Armour, and M. Zamir, Phys. Rev. E **70**, 051914 (2004).
[8] H. Rouse, *History of Hydraulics* (Dover Publications, New York, 1957).
[9] D. A. McDonald, *Blood Flow in Arteries* (Edward Arnold, London, 1974).
[10] C. G. Caro, T. J. Pedley, R. C. Schroter, and W. A. Seed, *The Mechanics of Circulation* (Oxford University Press, Oxford, 1978).
[11] W. R. Milnor, *Hemodynamics* (Williams and Wilkins, Baltimore, 1989).
[12] J. A. Armour, Can. J. Physiol. Pharmacol. **63**, 704 (1985).
[13] W. W. Nichols and W. F. O'Rourke, *McDonald's Blood Flow in Arteries* (Edward Arnold, London, 1998).